Title

Ultrasensitive Isothermal Detection of SARS-CoV–2 Based on Self-Priming Hairpin-Utilized Amplification of the G–Rich Sequence

Journal

Analytical Chemistry, 94(50)

ISSN

0003-2700

Authors

Li, Yan
Kim, Hansol
Ju, Yong
et al.

Publication Date

2022-12-20

DOI

10.1021/acs.analchem.2c03442

analytical chemistry

pubs.acs.org/ac

Article

Ultrasensitive Isothermal Detection of SARS-CoV-2 Based on Self-Priming Hairpin-Utilized Amplification of the G-Rich Sequence

Yan Li, Hansol Kim, Yong Ju, Yeonkyung Park, Taejoon Kang, Dongeun Yong, and Hyun Gyu Park*

Cite This: *Anal. Chem.* 2022, 94, 17448−17455

Read Online

ACCESS | Metrics & More | Article Recommendations | Supporting Information

ABSTRACT: The outbreak of the novel coronavirus disease 2019 (COVID-19) pandemic induced by severe acute respiratory syndrome coronavirus 2 (SARS-CoV-2) has caused millions of fatalities all over the world. Unquestionably, the effective and timely testing for infected individuals is the most imperative for the prevention of the ongoing pandemic. Herein, a new method was established for detecting SARS-CoV-2 based on the self-priming hairpin-utilized isothermal amplification of the G-rich sequence (SHIAG). In this strategy, the target RNA binding to the hairpin probe (HP) was uniquely devised to lead to the self-priming-mediated extension followed by the continuously repeated nicking and extension reactions, consequently generating abundant G-rich sequences from the intended reaction capable of producing fluorescence signals upon specifically interacting with thioflavin T (ThT). Based on the unique isothermal design concept, we successfully identified SARS-CoV-2 genomic RNA (gRNA) as low as 0.19 fM with excellent selectivity by applying only a single HP and further verified its practical diagnostic capability by reliably testing a total of 100 clinical specimens for COVID-19 with 100% clinical sensitivity and specificity. This study would provide notable insights into the design and evolution of new isothermal strategies for the sensitive and facile detection of SARS-CoV-2 under resource constraints.

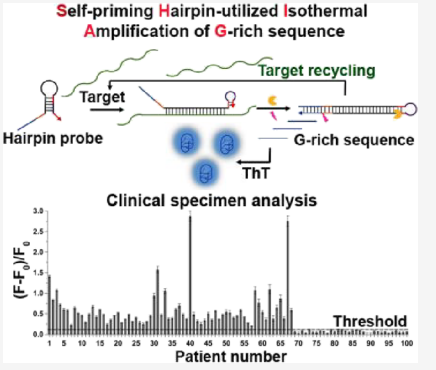

Since its appearance in late December 2019, coronavirus disease 2019 (COVID-19) caused by severe acute respiratory syndrome coronavirus 2 (SARS-CoV-2) has quickly transmitted worldwide. The World Health Organization (WHO) declared it as a global pandemic on 11 March 2020.[1] As of 30 May 2022, COVID-19 has infected and killed more than 520 and 6.2 million people worldwide, respectively,[2] posing unprecedented challenges to the global health and economy.

In comparison with severe acute respiratory syndrome coronavirus (SARS-CoV), Middle East respiratory syndrome coronavirus (MERS-CoV), or other epidemic human coronaviruses (HCoVs), SARS-CoV-2 virus exhibits increased human-to-human transmission and individuals carrying SARS-CoV-2 virus show no symptoms in many clinical cases, accelerating the viral transmission and significantly increasing its pandemic potential.[3−6] Furthermore, the SARS-CoV-2 virus has consistently mutated over time, resulting in the continual emergence of new SARS-CoV-2 variants showing higher transmissibility than the original virus,[7,8] which would make the prevention of the outbreak more challenging.[9] Most representatively, the Omicron variant spreads more easily than earlier variants including the Delta variant, and anyone with Omicron infection can spread the virus to others whether or not they have symptoms.[10−12]

Despite playing a predominant role in protecting individuals against severe forms of COVID-19, the coronavirus vaccines are not completely effective in preventing infection[13−15] and the Omicron variant is known to infect vaccinated people.[16−18] Therefore, timely testing COVID-19 cases through rapid and accurate methods and keeping infected patients under surveillance to curb further transmission are still of the most importance to control and manage the ongoing pandemic.[19,20]

The gold standard method for diagnosing COVID-19 is quantitative reverse transcription polymerase chain reaction (qRT-PCR) where the viral RNA is first converted to the complementary DNA (cDNA) succeeded by a qPCR process with the cDNA.[21−23] Despite its high clinical sensitivity and specificity, the qRT-PCR requires temperature cycling, takes a relatively lengthy testing period (3−4 h), and needs to be conducted in a centralized laboratory by an experienced operator, restricting its widespread applicability for point-of-care testing (POCT) purpose under resource constraints.[24−26]

Isothermal strategies to amplify nucleic acids could simplify and speed up the testing process, providing a compelling alternative to the conventional method based on thermocycling machine.[27−29] Since the early 1990s, dozens of isothermal amplification methods have been reported, such as Nucleic

Received: August 8, 2022
Accepted: November 28, 2022
Published: December 8, 2022

Scheme 1. Schematic Illustration of the SHIAG Reaction for Detecting SARS-CoV-2

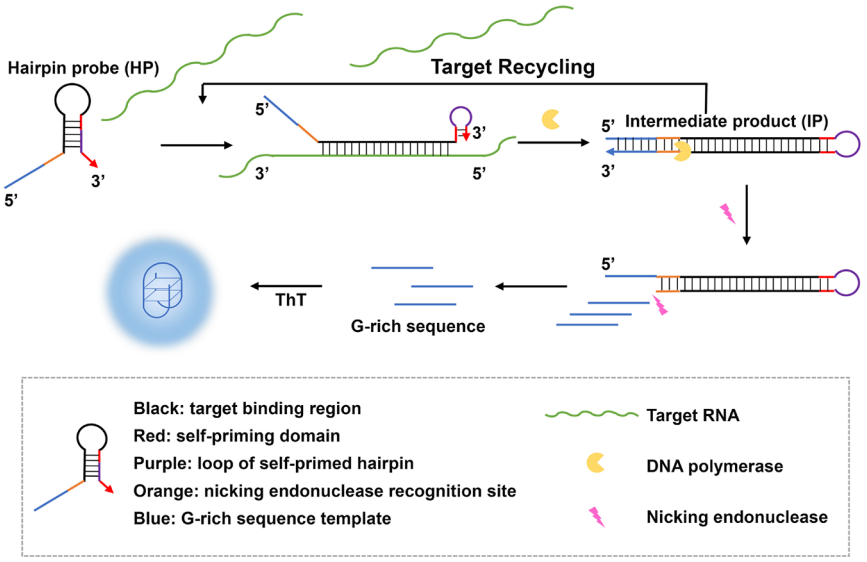

Acid Sequence Based Amplification (NASBA),[30,31] Strand Displacement Amplification (SDA),[32,33] Loop-mediated Isothermal Amplification (LAMP),[34,35] Rolling Circle Amplification (RCA),[36,37] target-induced Chain Amplification Reaction (CAR),[38] Nicking and Extension Chain Reaction System-based Amplification (NESBA),[39] and so on.[40−42] By taking advantage of the simplicity of apparatus and reaction procedure, most of the isothermal techniques showed great potential for POCT applications,[43] but several drawbacks including the requirement for multiple primers/probes,[44−46] relatively high reaction temperature,[47] and insufficient amplification efficiency[48−51] remain to be solved.

Based on this context, we herein developed a new technique to identify SARS-CoV-2 based on the self-priming hairpin-utilized isothermal amplification of the G-rich sequence (SHIAG). The self-priming hairpin probe (HP) was verified to enable the detection of synthetic DNA and RNA under the isothermal condition without any exogenous primers.[42] By making the most of the self-priming HP and the combined extension and nicking reactions to generate abundant G-rich sequences capable of producing fluorescence signals through specific interaction with thioflavin T (ThT), we successfully identified target SARS-CoV-2 genomic RNA (gRNA) as low as sub-femtomolar level with excellent selectivity in a one-pot reaction while applying only a single HP without any exogenous primers or prior labelings.

EXPERIMENTAL SECTION

Materials. All DNA oligonucleotides utilized in the current work were HPLC-purified and purchased from Bioneer (Daejeon, Korea). The target RNA oligonucleotide was RNase-free HPLC purified and purchased from Integrated DNA Technologies, Inc. (Coralville, IA, USA). All oligonucleotides are presented in Table S1. The gRNAs of SARS-CoV-2, HCoV-NL63, and MERS-CoV were supplied by the National Culture Collection for Pathogens (NCCP, Cheongju, Korea). The gRNAs of SARS-CoV and HCoV-HKU-1 were purchased from Intergrated DNA Technologies Inc. (Coralville, IA, USA) while the gRNAs of HCoV-OC43 and HCoV-229E were purchased from the Korea Bank for Pathogenic Viruses (KBPV, Seoul, Korea). Bst 2.0 WarmStart DNA polymerase (Bst, M0538S), Nt.BstNBI (R0607S), NEBuffer 3.1 (B7203S), ThermoPol reaction buffer (B9004S), and deoxynucleotide (dNTP) solution mix (N0447S) were purchased from New England Biolabs Inc. (Beverly, MA, USA). Diethyl pyrocarbonate (DEPC)-treated water (95284) and ThT (T3516) were purchased from Sigma-Aldrich (St. Louis, MO, USA). All other chemicals were of analytical grade and used as received without further purification.

SHIAG Reaction for SARS-CoV-2 Detection. Prior to use, 1 μM HP in 1× HP buffer (1 mM $MgSO_4$, 5 mM $(NH_4)_2SO_4$, 5 mM KCl, 7.5 mM $MgCl_2$, 47.5 mM Tris−HCl, 75 mM NaCl, 0.05% Triton X-100, 75 μg/mL BSA) was heated at 95 °C for 5 min and then cooled to 25 °C (0.1 °C/s) to ensure proper intramolecular folding and form a hairpin structure. The 20 μL SHIAG reaction solution was prepared to contain 0.5 μL of pretreated HP solution (1 μM), 1 μL of 10× ThermoPol reaction buffer (20 mM $MgSO_4$, 100 mM $(NH_4)_2SO_4$, 100 mM KCl, 200 mM Tris−HCl, 1% Triton X-100, pH 8.8), 1.5 μL of 10× NEBuffer 3.1 (100 mM $MgCl_2$, 500 mM Tris−HCl, 1 M NaCl, 1 mg/mL BSA, pH 7.9), 0.5 μL of dNTP (10 mM), 0.2 μL of Bst (8 U/μL), 0.16 μL of Nt.BstNBI nicking endonuclease (10 U/μL), 2 μL of ThT (250 μM), and 2 μL of target analyte, which was incubated at 37 °C for 60 min. From the reaction products, the fluorescence emission spectra in a range of 480−650 nm or the fluorescence emission intensities at 496 nm were monitored at an excitation wavelength of 440 nm by using a Tecan Infinite M200 Pro microplate reader (Männedorf, Switzerland) and 384-well Greiner Bio-One microplates (Ref. 781077, Courtaboeuf, France). To optimize reaction conditions, the fluorescence signal from ThT was recorded at an interval of 60 s at 37 °C by using a CFX Connect Real-Time System (Bio-Rad, CA, USA).

Polyacrylamide Gel Electrophoresis (PAGE) Analysis. For the PAGE assay, 10 μL of the reaction solution was resolved on 15% polyacrylamide gel at 120 V for 90 min using 1X TBE as the running buffer. After ethidium bromide (EtBr) staining, the gel was scanned using the ChemiDoc Imaging System (Bio-Rad, CA, USA).

Clinical Sample Testing with the SHIAG Reaction. Real clinical nasopharyngeal swab and sputum specimens (n = 100) were provided by Gyeongsang National University

https://doi.org/10.1021/acs.analchem.2c03442
Anal. Chem. 2022, 94, 17448−17455

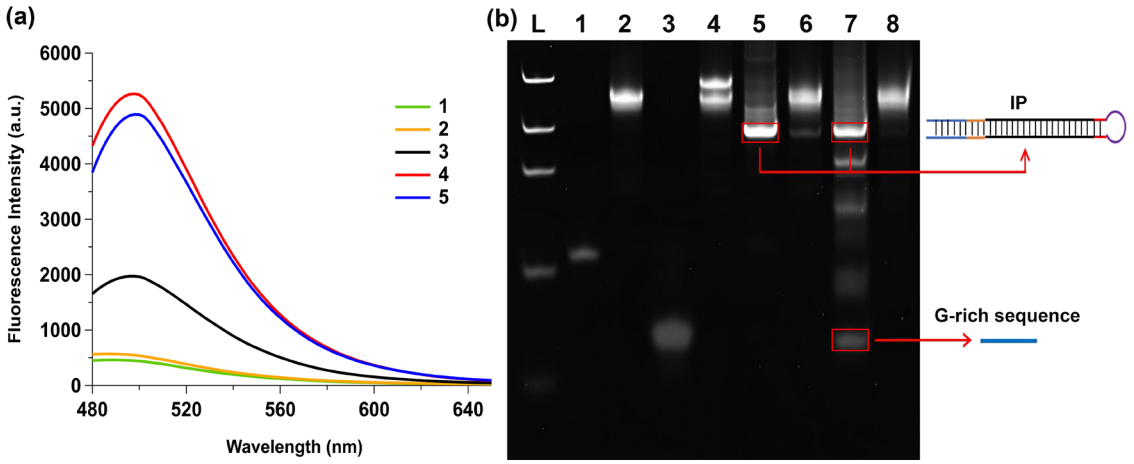

Figure 1. Feasibility of the SHIAG reaction for detecting SARS-CoV-2 RNA. (a) Fluorescence emission spectra of ThT under various combinations of reaction elements. (1) HP + Bst + ThT, (2) HP + target RNA + Bst + ThT, (3) HP + Bst + Nt.BstNBI + ThT, (4) HP + target RNA + Bst + Nt.BstNBI + ThT, (5) G-rich sequence + ThT. The final concentrations of target RNA, HP, Bst, Nt.BstNBI, and ThT are 1 nM, 25 nM, 0.08 U/μL, 0.08 U/μL, and 25 μM, respectively. (b) PAGE image of the SHIAG reaction products. L: ultra-low range ladder, (1) target RNA, (2) HP, (3) G-rich sequence, (4) HP + target RNA, (5) HP + target RNA + Bst, (6) HP + Bst, (7) HP + target RNA + Bst + Nt.BstNBI, (8) HP + Bst + Nt.BstNBI. The final concentrations of target RNA, HP, Bst, and Nt.BstNBI are 200 nM, 500 nM, 0.16 U/μL, and 0.16 U/μL, respectively. In this study, synthetic 40-mer RNA (Table S1) was used as target RNA.

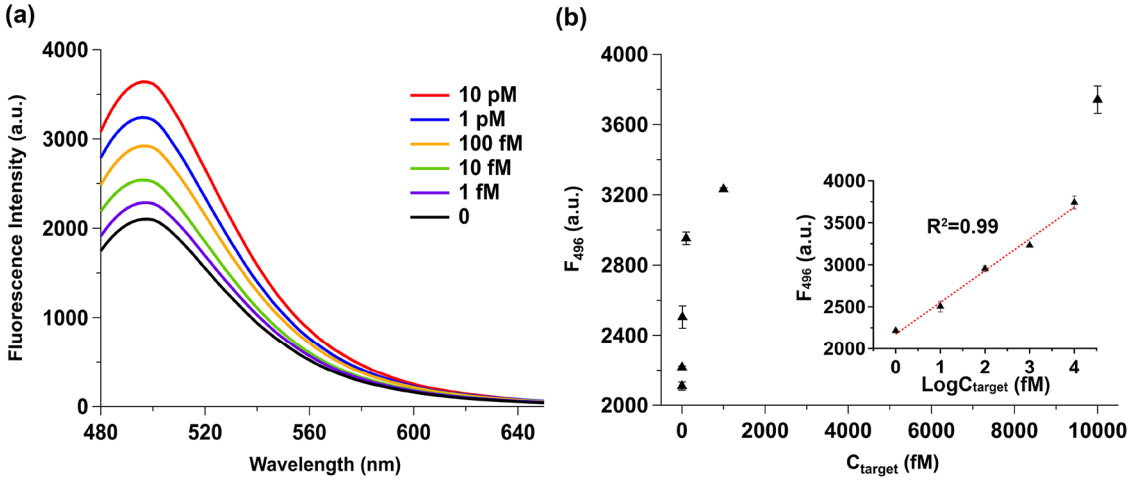

Figure 2. Sensitivity of the SHIAG reaction for detecting SARS-CoV-2 gRNA. (a) Fluorescence emission spectra and (b) fluorescence intensity at 496 nm (F_{496}) obtained from the SHIAG reactions with SARS-CoV-2 gRNA at various concentrations (0−10 pM). Inset in panel (b): linear relationship between F_{496} and logarithmic SARS-CoV-2 gRNA concentration (1 fM-10 pM). Error bars were calculated from triplicate experiments.

College of Medicine and Severance Hospital. The specimens were collected from individuals with suspected COVID-19 infection and stored in universal transport media at −70 °C. The protocols for these studies were reviewed and approved by the Institutional Review Board (IRB) of Gyeongsang National University College of Medicine (IRB approval number: 2020-10-002; Jinju, Korea) and Severance Hospital (IRB approval number: 4-2020-0465; Seoul, Korea). The gRNAs of the clinical specimens were extracted by using the AdvanSure Nucleic Acid R kit (LG chem, Seoul, Korea) and subjected to the SHIAG reaction according to the procedure as described above.

Clinical Specimen Analysis with qRT-PCR. For the clinical specimens provided by Gyeongsang National University College of Medicine, the qRT-PCR was carried out following the manufacturer's protocol of the Luna Universal One-Step RT-qPCR Kit (New England Biolabs Inc., Beverly, MA, USA). Reverse transcription (RT) was first conducted for 10 min at 55 °C, and the PCR was carried out for 1 min at 95 °C for initial denaturation, succeeded by 45 cycles of 10 s at 95 °C and 30 s at 60 °C. For the clinical samples acquired from Severance Hospital, the qRT-PCR was carried out following the manufacturer's protocol of the Allplex 2019-nCoV assay kit (Seegene Inc., Seoul, Korea). RT was first conducted for 20 min at 50 °C, and the PCR was carried out for 15 min at 95 °C for initial denaturation, succeeded by 45 cycles of 15 s at 94 °C and 30 s at 58 °C. Fluorescence signals of all specimens were monitored each cycle by using a CFX96 Real-Time System (Bio-Rad, CA, USA). The diagnostic call of each specimen was provided based on C_t values calculated by built-in system software.

RESULTS AND DISCUSSION

Working Principle of the SHIAG Reaction for Detecting SARS-CoV-2. The working principle of the SHIAG reaction for detecting SARS-CoV-2 is depicted in

https://doi.org/10.1021/acs.analchem.2c03442
Anal. Chem. 2022, 94, 17448−17455

Table 1. Comparison of SHIAG Method with Previous SARS-CoV-2 Detection Methods

methods	limit of detection (copies/μL)	limitations	reference
qRT-PCR	1.25	requirement for reverse-transcription step and thermal cycler	52
RT-LAMP	100	requirement for multiple primers	53,54
RT-LAMP	100/158	requirement for multiple primers	55
RT-LAMP	50	requirement for multiple primers	56
RT-LAMP	0.2−2	requirement for multiple primers	57
paper COV-ID	380	requirement for multiple primers and long preparation time	58
RT-LAMP-Cas12	10	requirement for multiple primers and CRISPR-Cas12a system	59
all-in-one dual CRISPR-Cas12a	5	requirement for multiple primers and CRISPR-Cas12a system	60
RT-LAMP-Cas13	25	requirement for multiple primers and CRISPR-Cas13a system	61
EXPAR	72.6	false-positive signal	62
CHA	2.5×10^7	low sensitivity	63
NISDA	10	labeling with fluorophore and quencher	64
SHIAG	114	marginal nonspecific signal	This work

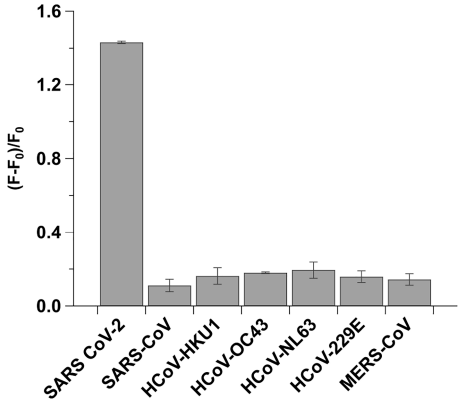

Figure 3. Specificity of the SHIAG reaction for detecting SARS-CoV-2 gRNA. Fluorescence enhancement ($(F - F_0)/F_0$, where the fluorescence intensities at 496 nm without and with gRNAs are indicated as F_0 and F, respectively) obtained from the SHIAG reactions with SARS-CoV-2 gRNA or other non-target gRNAs including SARS-CoV gRNA, HCoV-HKU-1 gRNA, HCoV-OC43 gRNA, HCoV-NL63 gRNA, HCoV-229E gRNA, and MERS-CoV gRNA. The concentration of each type of gRNA is 1 pM. Error bars were calculated from triplicate experiments.

Scheme 1. The core element actuating the SHIAG reaction is the uniquely designed HP containing four functional domains: target binding region in stem and loop (black domain), self-priming region along the 3′ end (red and purple domain), and nicking endonuclease recognition site (orange domain) and G-rich sequence template at the 5′ overhang (blue domain).

In the absence of target RNA, HP maintains its stable hairpin structure in the solution as the self-primer region is caged within the hairpin stem region, and no following enzymatic reactions proceed. In the presence of target RNA, however, the target binding region of HP hybridizes with target RNA, which would disrupt its hairpin structure and rearrange its 3′-end to be self-primed. The self-primed 3′ end is then extended by DNA polymerase to produce a dsDNA intermediate product (IP). During the extension, target RNA is concomitantly displaced and recycled to open another HP. Owing to the presence of a nicking endonuclease recognition site within IP, continuously repeated nicking and extension reactions would be promoted through the combined activity of nicking endonuclease and DNA polymerase, consequently generating abundant G-rich sequences. The G-rich sequences finally produce the significantly enhanced fluorescence signals by forming G-quadruplex structures and specifically interacting with ThT, which can be used to identify target RNAs.

Feasibility of the SHIAG Reaction for Detecting SARS-CoV-2. The detection feasibility of the SHIAG reaction was verified by recording the fluorescence emission spectra obtaining from the reactions under diverse combinations of reaction elements (Figure 1a). First, when the sample contained neither target RNA and nicking endonuclease, the HP just kept its initial structure and no following enzymatic reactions proceeded as evidenced by a very negligible fluorescence signal (curve 1). Even when target RNA was additionally applied, the fluorescence signal remained negligible in the absence of nicking endonuclease (curve 2) because free G-rich sequences cannot be produced from the IP without the action of nicking endonuclease. Most importantly, significant fluorescence enhancement was detected when all reaction elements including HP, nicking endonuclease, and DNA polymerase were applied to the positive sample containing target RNA (curve 4), which was quite coincident with the case where the synthetic G-rich sequences were externally introduced to ThT (curve 5). Notably, a marginal nonspecific fluorescence signal was detected from the negative sample without target RNA but containing all the reaction elements, indicating that the HP might be slightly rearranged to actuate the reaction even without the interaction of target RNA, which could be a limitation of the proposed strategy. Nevertheless, the specific signal obtained from target RNA was far greater and more than enough to be clearly discriminated from the nonspecific signal. The results indicate that target RNA is exclusively responsible to initiate the reaction, and nicking endonuclease and also DNA polymerase are imperative to promote the whole reaction to produce G-rich sequences, which would lead to significantly enhanced fluorescence signals through specific interaction with ThT.

We additionally carried out the PAGE assay for the reaction elements and products generated from the SHIAG reaction (Figure 1b) to further support the results from the fluorescence emission spectra. First, the intense band corresponding to the IP was correctly observed when the samples contained the three elements required for the production of IP, such as HP, target RNA, and DNA polymerase (lane 5 and lane 7). On the other hand, the initially applied HP was just kept unextended and no band for the IP was observed when either DNA polymerase (lane 4) or target RNA (lane 6 and lane 8) was omitted. Most importantly, an intense band corresponding to the free G-rich sequence, the final product of the SHIAG reaction was clearly observed only from the solution comprising all the reaction elements including HP, nicking endonuclease, DNA polymerase, and target RNA (lane 7). Collectively, these results verify that the SHIAG reaction is efficiently actuated by target RNAs and works effectively as envisioned by the mechanism in Scheme 1.

Sensitivity of the SHIAG Reaction for SARS-CoV-2 Detection. To maximize the performance of the SHIAG reaction, we optimized the reaction conditions by monitoring

https://doi.org/10.1021/acs.analchem.2c03442
Anal. Chem. 2022, 94, 17448−17455

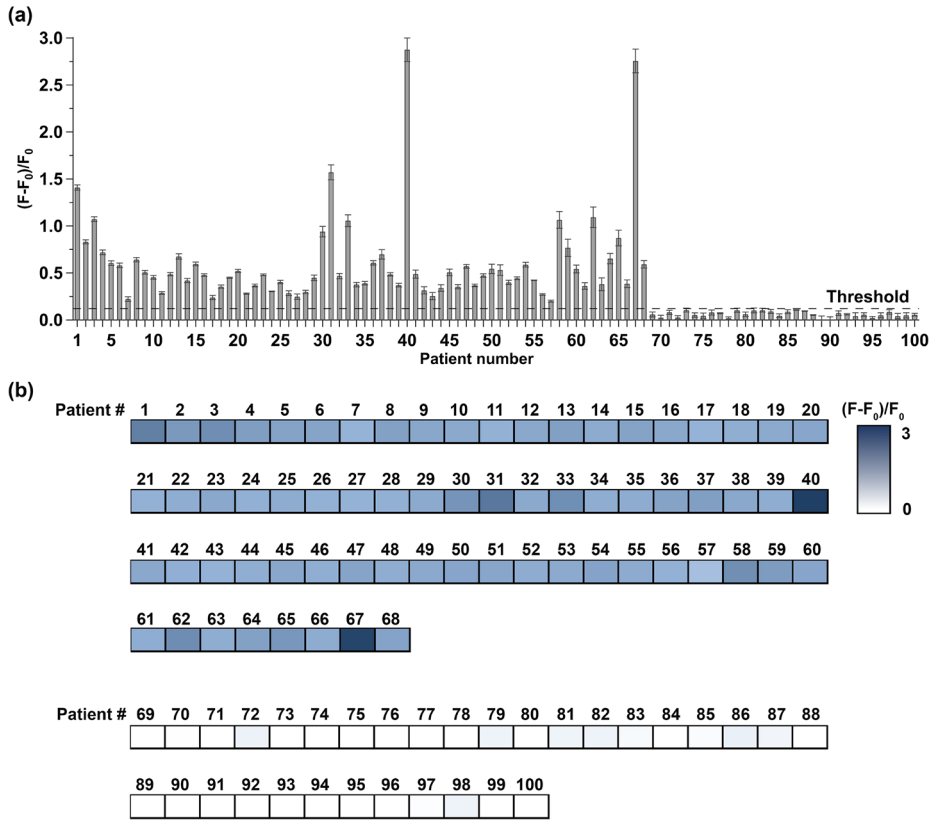

Figure 4. Clinical specimen analysis with the SHIAG reaction. (a) Fluorescence enhancement ($(F - F_0)/F_0$, where the fluorescence intensities at 496 nm without and with gRNAs extracted from clinical specimens are indicated as F_0 and F, respectively) obtained from the SHIAG reactions with 100 nasopharyngeal swab and sputum specimens. The threshold is calculated as background + 5SD, where the background represents the average fluorescence enhancement of the blank and SD represents the standard deviation of the blank, which was used to call specimens positive (1−68) or negative (69−100). Error bars were calculated from triplicate experiments. (b) Heat map of $(F - F_0)/F_0$ values from testing on 100 clinical specimens using the SHIAG reaction.

Table 2. Clinical Specimen Analysis for 68 Positive and 32 Negative Cases with qRT-PCR and the SHIAG Method

diagnostic parameter		qRT-RCR	SHIAG
positive	true	68	68
	false		
negative	true	32	32
	false		
sensitivity (%)		100	100
(95% CI%)[a]		(94.72−100)	(94.72−100)
specificity (%)		100	100
(95% CI%)[a]		(89.11−100)	(89.11−100)

[a]Confidence interval (MedCalc software, version 20.027).

the fluorescence enhancement generated from the SHIAG reactions as $(F - F_0)/F_0$, where the fluorescence intensities at 496 nm of the reaction solutions without and with target RNA are indicated as F_0 and F, respectively. As shown in Figures S1−S7, 37 °C, 25 nM HP, 0.5× ThermoPol reaction buffer, 0.75× NEBuffer 3.1, 0.08 U/μL of Bst, and 0.08 U/μL of Nt.BstNBI, 60 min were optimal, which were employed throughout further assays.

To evaluate the sensitivity of the SHIAG reaction, the reaction was conducted by employing target gRNA at various concentrations (0−10 pM) and the resulting fluorescence signals were analyzed. As presented in Figure 2a, the fluorescence intensity enhanced as concentration of SARS-CoV-2 gRNA increased, and an excellent linear relationship (F_{496} = 377.63 log(C_{target}(fM)) + 2173.9, R^2 = 0.99) was detected in the range of 1 fM to 10 pM when fluorescence intensity at 496 nm (F_{496}) was plotted as a function of logarithmic SARS-CoV-2 gRNA concentration (Figure 2b), revealing that the proposed method is fully capable for the quantitative identification of SARS-CoV-2 gRNA. The limit of detection (LOD) was determined to be 0.19 fM (114 copies/μL) based on the equation: LOD = 3σ/S, where the standard deviation of the blank and the slope of the calibration line are indicated as σ and S, respectively. The LOD is comparable to those from previous SARS-CoV-2 detection methods (Table 1). As shown in Table 1, the SHIAG reaction is capable of SARS-CoV-2 detection without involving any exogenous primers, multiple probes, prior labelings, and thermal cycling, remarkably simplifying the detection procedure and presenting prominent advantages over previous methods.

Specificity of the SHIAG Reaction for SARS-CoV-2 Detection. The detection specificity of the SHIAG reaction for SARS-CoV-2 detection was next analyzed through comparing the fluorescence enhancement obtained from target SARS-CoV-2 gRNA with those from other types of HCoV gRNAs including SARS-CoV gRNA, HCoV-HKU-1 gRNA, HCoV-OC43 gRNA, HCoV-NL63 gRNA, HCoV-229E gRNA, and MERS-CoV gRNA. As shown in Figure 3, significantly enhanced fluorescence was examined only from target SARS-CoV-2 gRNA, while only negligible fluorescence

https://doi.org/10.1021/acs.analchem.2c03442
Anal. Chem. 2022, 94, 17448−17455

enhancement was observed from all non-target gRNAs. The results verify that the specific binding between the HP and target RNA needs to be essentially proceeded to properly promote the SHIAG reaction, ensuring the excellent specificity of the SHIAG reaction only toward the target RNA.

Clinical Applicability of the SHIAG Reaction. The clinical applicability of the SHIAG reaction was lastly demonstrated by monitoring the fluorescence signals resulting from the reactions with gRNAs extracted from real clinical nasopharyngeal swab and sputum specimens (n = 100). As shown in Figure 4a, 68 specimens among total 100 specimens produced significant fluorescence increases from the SHIAG reactions and were called positive based on the general threshold guideline of background + 5SD, where the background and SD represent the average fluorescence enhancement of the blank and the standard deviation of the blank, respectively.[65] The remaining 32 specimens produced only very negligible fluorescence increases and were called negative. All the fluorescence increase $(F - F_0)/F_0$ values for 100 clinical specimens were displayed in the corresponding heat map to more vividly visualize the results by color (Figure 4b), which further manifests the clear discrimination of positive specimens against negative specimens. We also conducted the testing for the same 100 clinical specimens but using the current gold standard qRT-PCR method. As the results presented in Table 2 and Table S2, the qRT-PCR identified the same 68 specimens as positive and the same 32 specimens as negative, which fully agreed with the SHIAG method. By using the diagnostic call from qRT-PCR as reference, the SHIAG reaction successfully confirmed all the 100 clinical specimens with 100% clinical sensitivity and specificity, verifying that the proposed strategy could reliably test COVID-19 specimens in practical clinical applications and could replace the current qRT-PCR.

CONCLUSIONS

The development of testing methods to accurately and rapidly identify infected individuals at scale is an urgent goal to efficiently contain the current COVID-19 pandemic. We herein proposed a new isothermal amplification strategy termed the SHIAG reaction and successfully identified SARS-CoV-2 gRNA as low as 0.19 fM (114 copies/μL) with excellent selectivity. The clinical capability of the SHIAG reaction was further verified by reliably testing 100 clinical specimens with 100% clinical sensitivity and specificity, confirming its robust clinical applicability.

The SHIAG reaction described in this work yields several distinct advantages for nucleic acid detection. First, due to the unique design of the HP possessing the elemental fractions to enable from the initial self-priming to the final signaling, the final fluorescent signals could be produced instantly upon its binding to target RNA without involving any exogenous primers but only a single HP is enough to actuate the whole isothermal process. Second, the SHIAG reaction continuously displaces and recycles the bound target RNA, consequently achieving ultrasensitive detection for target RNA even under the isothermal condition. Third, the final G-rich sequences produced through continuously repeated nicking and extension reactions produce the signal just by interacting with ThT, eliminating the need for any prior labelings. This technique could be generally applied to identify other pathogens by simply redesigning the flexible HP sequence according to the target and thereby has a great potential to be a new robust isothermal tool enabling facile molecular testing of new emerging pathogens.

ASSOCIATED CONTENT

Supporting Information

The Supporting Information is available free of charge at https://pubs.acs.org/doi/10.1021/acs.analchem.2c03442.

Sequence information (Table S1); qRT-PCR results of clinical samples (Table S2); optimization of the SARS-CoV-2 detection method (Figures S1−S7) (PDF)

AUTHOR INFORMATION

Corresponding Author

Hyun Gyu Park − *Department of Chemical and Biomolecular Engineering (BK21 Four), Korea Advanced Institute of Science and Technology (KAIST), Daejeon 34141, Republic of Korea;* orcid.org/0000-0001-9978-3890; Email: hgpark@kaist.ac.kr

Authors

Yan Li − *Department of Chemical and Biomolecular Engineering (BK21 Four), Korea Advanced Institute of Science and Technology (KAIST), Daejeon 34141, Republic of Korea*

Hansol Kim − *Department of Chemical and Biomolecular Engineering (BK21 Four), Korea Advanced Institute of Science and Technology (KAIST), Daejeon 34141, Republic of Korea*

Yong Ju − *Department of Chemical and Biomolecular Engineering (BK21 Four), Korea Advanced Institute of Science and Technology (KAIST), Daejeon 34141, Republic of Korea*

Yeonkyung Park − *Department of Chemical and Biomolecular Engineering (BK21 Four), Korea Advanced Institute of Science and Technology (KAIST), Daejeon 34141, Republic of Korea*

Taejoon Kang − *Bionanotechnology Research Center, Korea Research Institute of Bioscience and Biotechnology (KRIBB), Daejeon 34141, Republic of Korea; School of Pharmacy, Sungkyunkwan University, Suwon, Gyeonggi-do 16419, Republic of Korea;* orcid.org/0000-0002-5387-6458

Dongeun Yong − *Department of Laboratory Medicine and Research Institute of Bacterial Resistance, Yonsei University College of Medicine, Seoul 03722, Republic of Korea*

Complete contact information is available at: https://pubs.acs.org/10.1021/acs.analchem.2c03442

Author Contributions

The manuscript was written through contributions of all authors. All authors have given approval to the final version of the manuscript.

Notes

The authors declare no competing financial interest.

ACKNOWLEDGMENTS

This research was supported by the Mid-career Researcher Support Program of the National Research Foundation (NRF) funded by MSIT of Korea (NRF-2021R1A2B5B03001739) and KRIBB Research Initiative Program (1711134081). This research was also supported by the Korean National Police Agency (Project Name: Development of visualization technol-

ogy for biological evidence in crime scenes based on nanobiotechnology/Project Number: PA-K000001-2019-101).

REFERENCES

(1) WHO-Statement. *WHO Timeline - COVID-19*. 2020. https://www.who.int/news-room/detail/27-04-2020-who-timeline---covid-19 (accessed 2020 April).
(2) WHO. *WHO Coronavirus (COVID-19) Dashboard*. 2022. https://covid19.who.int/ (accessed 2022 April).
(3) Petersen, E.; Koopmans, M.; Go, U.; Hamer, D. H.; Petrosillo, N.; Castelli, F.; Storgaard, M.; Al Khalili, S.; Simonsen, L. *Lancet Infect. Dis.* **2020**, *20*, e238−e244.
(4) Abdelrahman, Z.; Li, M.; Wang, X. *Front. Immunol.* **2020**, *11*, No. 552909.
(5) Shang, J.; Wan, Y.; Luo, C.; Ye, G.; Geng, Q.; Auerbach, A.; Li, F. *Proc. Natl. Acad. Sci. U. S. A.* **2020**, *117*, 11727−11734.
(6) Mao, K.; Zhang, H.; Yang, Z. *Environ. Sci. Technol.* **2020**, *54*, 3733−3735.
(7) Campbell, F.; Archer, B.; Laurenson-Schafer, H.; Jinnai, Y.; Konings, F.; Batra, N.; Pavlin, B.; Vandemaele, K.; Van Kerkhove, M. D.; Jombart, T.; et al. *Eurosurveillance* **2021**, *26*, No. 2100509.
(8) Lyngse, F. P.; Molbak, K.; Skov, R. L.; Christiansen, L. E.; Mortensen, L. H.; Albertsen, M.; Moller, C. H.; Krause, T. G.; Rasmussen, M.; Michaelsen, T. Y.; et al. *Nat. Commun.* **2021**, *12*, 7251.
(9) WHO-Departmental News. *Tracking SARS-CoV-2 variants*. 2022. https://www.who.int/en/activities/tracking-SARS-CoV-2-variants/ (accessed 2022 April).
(10) Callaway, E.; Ledford, H. *Nature* **2021**, *600*, 197−199.
(11) Kupferschmidt, K.; Vogel, G. *Science* **2021**, *374*, 1304−1305.
(12) CDC. *Omicron variant: what you need to know*. 2022. https://www.cdc.gov/coronavirus/2019-ncov/variants/omicron-variant.html (accessed 2022 March).
(13) Edwards, K. M.; Orenstein, W. A. *COVID-19: Vaccines to prevent SARS-CoV-2 infection*. 2022. https://www.uptodate.com/contents/covid-19-vaccines-to-prevent-sars-cov-2-infection (accessed 2022 April).
(14) Maragakis, L.; Kelen, G. D. *Breakthrough infections: Coronavirus after vaccination*. 2021. https://www.hopkinsmedicine.org/health/conditions-and-diseases/coronavirus/breakthrough-infections-coronavirus-after-vaccination (accessed 2021 November).
(15) WHO-Science Conversation. *Can I get infected after vaccination?* 2021. https://www.who.int/emergencies/diseases/novel-coronavirus-2019/media-resources/science-in-5/episode-49-can-i-get-infected-after-vaccination (accessed 2021 August).
(16) Garcia-Beltran, W. F.; St Denis, K. J.; Hoelzemer, A.; Lam, E. C.; Nitido, A. D.; Sheehan, M. L.; Berrios, C.; Ofoman, O.; Chang, C. C.; Hauser, B. M.; et al. *Cell* **2022**, *185*, 457−466.
(17) Kuhlmann, C.; Mayer, C. K.; Claassen, M.; Maponga, T.; Burgers, W. A.; Keeton, R.; Riou, C.; Sutherland, A. D.; Suliman, T.; Shaw, M. L.; et al. *Lancet* **2022**, *399*, 625−626.
(18) Zhou, R.; To, K. K.; Peng, Q.; Chan, J. M.; Huang, H.; Yang, D.; Lam, B. H.; Chuang, V. W.; Cai, J. P.; Liu, N.; Au, K. K.; Tsang, O. T.; Yuen, K. Y.; Chen, Z. *Clin. Transl. Med.* **2022**, *12*, No. e720.
(19) Hellewell, J.; Abbott, S.; Gimma, A.; Bosse, N. I.; Jarvis, C. I.; Russell, T. W.; Munday, J. D.; Kucharski, A. J.; Edmunds, W. J.; Centre for the Mathematical Modelling of Infectious Diseases Covid-19 Working Group; et al. *Lancet Glob. Health* **2020**, *8*, e488−e496.
(20) Taleghani, N.; Taghipour, F. *Biosens. Bioelectron.* **2021**, *174*, No. 112830.
(21) Binnicker, M. J. *Clin. Chem.* **2020**, *66*, 664−666.
(22) Corman, V. M.; Landt, O.; Kaiser, M.; Molenkamp, R.; Meijer, A.; Chu, D. K.; Bleicker, T.; Brunink, S.; Schneider, J.; Schmidt, M. L.; et al. *Eurosurveillance* **2020**, *25*, 2000045.
(23) Freeman, W. M.; Walker, S. J.; Vrana, K. E. *BioTechniques* **1999**, *26*, 112−125 124-125.
(24) Tang, Y. W.; Schmitz, J. E.; Persing, D. H.; Stratton, C. W. *J. Clin. Microbiol.* **2020**, *58*, e00512−e00520.
(25) Carter, L. J.; Garner, L. V.; Smoot, J. W.; Li, Y.; Zhou, Q.; Saveson, C. J.; Sasso, J. M.; Gregg, A. C.; Soares, D. J.; Beskid, T. R.; et al. *ACS Cent. Sci.* **2020**, *6*, 591−605.
(26) Lee, H. N.; Lee, J.; Kang, Y. K.; Lee, J. H.; Yang, S.; Chung, H. J. *BioChip J.* **2022**, 1−10.
(27) Obande, G. A.; Banga Singh, K. K. *Infect. Drug Resist.* **2020**, *Volume 13*, 455−483.
(28) Zhu, X.; Wang, X.; Han, L.; Chen, T.; Wang, L.; Li, H.; Li, S.; He, L.; Fu, X.; Chen, S.; et al. *Biosens. Bioelectron.* **2020**, *166*, No. 112437.
(29) Subsoontorn, P.; Lohitnavy, M.; Kongkaew, C. *Sci. Rep.* **2020**, *10*, 22349.
(30) Guatelli, J. C.; Whitfield, K. M.; Kwoh, D. Y.; Barringer, K. J.; Richman, D. D.; Gingeras, T. R. *Proc. Natl. Acad. Sci. U. S. A.* **1990**, *87*, 1874−1878.
(31) Compton, J. *Nature* **1991**, *350*, 91−92.
(32) Walker, G. T.; Little, M. C.; Nadeau, J. G.; Shank, D. D. *Proc. Natl. Acad. Sci. U. S. A.* **1992**, *89*, 392−396.
(33) Walker, G. T.; Fraiser, M. S.; Schram, J. L.; Little, M. C.; Nadeau, J. G.; Malinowski, D. P. *Nucleic Acids Res.* **1992**, *20*, 1691−1696.
(34) Notomi, T.; Okayama, H.; Masubuchi, H.; Yonekawa, T.; Watanabe, K.; Amino, N.; Hase, T. *Nucleic Acids Res.* **2000**, *28*, E63.
(35) Hong, T. C.; Mai, Q. L.; Cuong, D. V.; Parida, M.; Minekawa, H.; Notomi, T.; Hasebe, F.; Morita, K. *J. Clin. Microbiol.* **2004**, *42*, 1956−1961.
(36) Fire, A.; Xu, S. Q. *Proc. Natl. Acad. Sci. U. S. A.* **1995**, *92*, 4641−4645.
(37) Harcourt, E. M.; Kool, E. T. *Nucleic Acids Res.* **2012**, *40*, e65.
(38) Kim, H. Y.; Song, J.; Park, H. G. *Biosens. Bioelectron.* **2021**, *178*, No. 113048.
(39) Ju, Y.; Kim, J.; Park, Y.; Lee, C. Y.; Kim, K.; Hong, K. H.; Lee, H.; Yong, D.; Park, H. G. *Biosens. Bioelectron.* **2022**, *196*, No. 113689.
(40) Song, J.; Kim, H. Y.; Kim, S.; Jung, Y.; Park, H. G. *Biosens. Bioelectron.* **2021**, *178*, No. 113051.
(41) Ju, Y.; Kim, H. Y.; Ahn, J. K.; Park, H. G. *Nanoscale* **2021**, *13*, 10785−10791.
(42) Song, J. Y.; Jung, Y.; Lee, S.; Park, H. G. *Anal. Chem.* **2020**, *92*, 10350−10356.
(43) Ganguli, A.; Ornob, A.; Yu, H.; Damhorst, G. L.; Chen, W.; Sun, F.; Bhuiya, A.; Cunningham, B. T.; Bashir, R. *Biomed. Microdevices* **2017**, *19*, 73.
(44) Dhama, K.; Karthik, K.; Chakraborty, S.; Tiwari, R.; Kapoor, S.; Kumar, A.; Thomas, P. *Pak. J. Biol. Sci.* **2014**, *17*, 151−166.
(45) Dirks, R. M.; Pierce, N. A. *Proc. Natl. Acad. Sci. U. S. A.* **2004**, *101*, 15275−15278.
(46) Yin, P.; Choi, H. M.; Calvert, C. R.; Pierce, N. A. *Nature* **2008**, *451*, 318−322.
(47) Mori, Y.; Notomi, T. *J. Infect. Chemother.* **2009**, *15*, 62−69.
(48) Watts, M. R.; James, G.; Sultana, Y.; Ginn, A. N.; Outhred, A. C.; Kong, F.; Verweij, J. J.; Iredell, J. R.; Chen, S. C.; Lee, R. *Am. J. Trop. Med. Hyg.* **2014**, *90*, 306−311.
(49) Deiman, B.; van Aarle, P.; Sillekens, P. *Mol. Biotechnol.* **2002**, *20*, 163−180.
(50) Loens, K.; Ursi, D.; Ieven, M.; van Aarle, P.; Sillekens, P.; Oudshoorn, P.; Goossens, H. *J. Clin. Microbiol.* **2002**, *40*, 1339−1345.
(51) Jang, M.; Kim, S. *BioChip J.* **2022**, *16*, 326−333.
(52) Farfour, E.; Lesprit, P.; Visseaux, B.; Pascreau, T.; Jolly, E.; Houhou, N.; Mazaux, L.; Asso-Bonnet, M.; Vasse, M.; Marc Vasse on behalf of the SARS-CoV-2 Foch Hospital study group. *Eur. J. Clin. Microbiol. Infect. Dis.* **2020**, *39*, 1997−2000.
(53) Baek, Y. H.; Um, J.; Antigua, K. J. C.; Park, J. H.; Kim, Y.; Oh, S.; Kim, Y. I.; Choi, W. S.; Kim, S. G.; Jeong, J. H.; Chin, B. S.; Nicolas, H. D. G.; Ahn, J. Y.; Shin, K. S.; Choi, Y. K.; Park, J. S.; Song, M. S. *Emerg. Microbes. Infect.* **2020**, *9*, 998−1007.
(54) Mautner, L.; Baillie, C. K.; Herold, H. M.; Volkwein, W.; Guertler, P.; Eberle, U.; Ackermann, N.; Sing, A.; Pavlovic, M.; Goerlich, O.; et al. *Virol. J.* **2020**, *17*, 160.

https://doi.org/10.1021/acs.analchem.2c03442
Anal. Chem. 2022, 94, 17448−17455

(55) Odiwuor, N.; Xiong, J.; Ogolla, F.; Hong, W.; Li, X. H.; Khan, F. M.; Wang, N. U.; Yu, J. P.; Wei, H. P. *Anal. Chim. Acta* **2022**, *1200*, No. 339590.
(56) Rabe, B. A.; Cepko, C. *Proc. Natl. Acad. Sci. U. S. A.* **2020**, *117*, 24450−24458.
(57) Song, J.; El-Tholoth, M.; Li, Y.; Graham-Wooten, J.; Liang, Y.; Li, J.; Li, W.; Weiss, S. R.; Collman, R. G.; Bau, H. H. *Anal. Chem.* **2021**, *93*, 13063−13071.
(58) Warneford-Thomson, R.; Shah, P. P.; Lundgren, P.; Lerner, J.; Morgan, J.; Davila, A.; Abella, B. S.; Zaret, K.; Schug, J.; Jain, R.; et al. *Elife* **2022**, *11*, No. e69949.
(59) Broughton, J. P.; Deng, X. D.; Yu, G. X.; Fasching, C. L.; Servellita, V.; Singh, J.; Miao, X.; Streithorst, J. A.; Granados, A.; Sotomayor-Gonzalez, A.; et al. *Nat. Biotechnol.* **2020**, *38*, 870−874.
(60) Ding, X.; Yin, K.; Li, Z. Y.; Lalla, R. V.; Ballesteros, E.; Sfeir, M. M.; Liu, C. C. *Nat. Commun.* **2020**, *11*, 4711.
(61) Agrawal, S.; Fanton, A.; Chandrasekaran, S. S.; Charrez, B.; Escajeda, A. M.; Son, S.; McIntosh, R.; Bhuiya, A.; de Leon Derby, M. D.; Switz, N. A.; et al. Rapid, point-of-care molecular diagnostics with Cas13. *medRxiv* **2021**.
(62) Carter, J. G.; Iturbe, L. O.; Duprey, J. L. H. A.; Carter, I. R.; Southern, C. D.; Rana, M.; Whalley, C. M.; Bosworth, A.; Beggs, A. D.; Hicks, M. R.; et al. *Proc. Natl. Acad. Sci. U. S. A.* **2021**, *118*, No. e2100347118.
(63) Do, J. Y.; Jeong, J. Y.; Hong, C. A. *Talanta* **2021**, *233*, No. 122505.
(64) Mohammadniaei, M.; Zhang, M.; Ashley, J.; Christensen, U. B.; Friis-Hansen, L. J.; Gregersen, R.; Lisby, J. G.; Benfield, T. L.; Nielsen, F. E.; Henning Rasmussen, J.; et al. *Nat. Commun.* **2021**, *12*, 5089.
(65) Fotis, C.; Meimetis, N.; Tsolakos, N.; Politou, M.; Akinosoglou, K.; Pliaka, V.; Minia, A.; Terpos, E.; Trougakos, I. P.; Mentis, A.; et al. *Sci. Rep.* **2021**, *11*, 6614.

https://doi.org/10.1021/acs.analchem.2c03442
Anal. Chem. 2022, 94, 17448−17455